Direct Intracochlear Acoustic Stimulation Using a PZT Microactuator

Chuan Luo[1,2], Irina Omelchenko[3], Robert Manson[1],
Carol Robbins[3], Elizabeth C. Oesterle[3], Guo Zhong Cao[4],
I.Y. Shen[1], and Clifford R. Hume[3,5]

Abstract

Combined electric and acoustic stimulation has proven to be an effective strategy to improve hearing in some cochlear implant users. We describe an acoustic microactuator to directly deliver stimuli to the perilymph in the scala tympani. The 800 μm by 800 μm actuator has a silicon diaphragm driven by a piezoelectric thin film (e.g., lead-zirconium-titanium oxide or PZT). This device could also be used as a component of a bimodal acoustic-electric electrode array. In the current study, we established a guinea pig model to test the actuator for its ability to deliver auditory signals to the cochlea in vivo. The actuator was placed through the round window of the cochlea. Auditory brainstem response (ABR) thresholds, peak latencies, and amplitude growth were calculated for an ear canal speaker versus the intracochlear actuator for tone burst stimuli at 4, 8, 16, and 24 kHz. An ABR was obtained after removal of the probe to assess loss of hearing related to the procedure. In some animals, the temporal bone was harvested for histologic analysis of cochlear damage. We show that the device is capable of stimulating ABRs in vivo with latencies and growth functions comparable to stimulation in the ear canal. Further experiments will be necessary to evaluate the efficiency and safety of this modality in long-term auditory stimulation and its ability to be integrated with conventional cochlear implant arrays.

Keywords

Cochlear implant, hearing aid, PZT, cochlea, piezoelectric, perilymph, hybrid, electroacoustic

Introduction

Hearing loss is one of the most common sensory disorders, and it is estimated that 15% of the adult U.S. population have some trouble hearing that affects quality of life (Blackwell, Lucas, & Clarke, 2014). Despite advances in hearing aids and cochlear implants over the past decades, a significant proportion of hearing-impaired individuals are dissatisfied with their devices (Kochkin, 2010). As hearing loss develops, individuals often first lose their high-frequency hearing associated with changes in the basal region of the cochlea. With further progression, the loss may also involve lower frequency, more apical, regions. A gradual evolution of cochlear implant technology and surgical technique has allowed for increased preservation of residual hearing and electroacoustic (EAS) or *hybrid* stimulation of the same ear with both acoustic and electrical stimuli (Gantz & Turner, 2003; Gstoettner et al., 2004; Woodson, Reiss, Turner, Gfeller, & Gantz, 2010). In this configuration, a shortened, minimally traumatic, cochlear implant electrode array is inserted into the basal cochlea to stimulate the high-frequency region, while a conventional acoustic hearing aid is used to deliver amplified acoustic stimulation. The combination of residual

[1]Department of Mechanical Engineering, University of Washington, Seattle, WA, USA
[2]Department of Precision Instruments, Tsinghua University, Beijing, China
[3]Virginia Merrill Bloedel Hearing Research Center, Department of Otolaryngology–Head and Neck Surgery, University of Washington, Seattle, WA, USA
[4]Department of Materials Science, University of Washington, Seattle, WA, USA
[5]VA Puget Sound, Seattle, WA, USA

Corresponding author:
I.Y. Shen, Department of Mechanical Engineering, University of Washington, Box 352600, Seattle, WA 98195-2600, USA.
Email: ishen@u.washington
Clifford R. Hume, Department of Otolaryngology–Head and Neck Surgery, University of Washington, 1959 NE Pacific, Virginia Merril Bloedel, Box 357923, Seattle WA 98195, USA.
Email: hume@uw.edu

low-frequency hearing and high-frequency electrical stimulation via cochlear implants yields improvement in auditory performance, including more appreciation of aesthetic qualities of sound and speech, better performance in background noise, and improved sound localization compared with hearing aids or cochlear implants alone (Irving et al., 2014; Talbot & Hartley, 2008; Turner & Gantz, 2012). While a significant number of patients eventually lose some of their residual hearing, it is expected that hearing preservation will continue to improve with better understanding of its causes.

Although the extent of sound processing integration is increasing, current strategies for EAS rely on separate components for the electrical stimulation (via an intracochlear electrode) and acoustic stimulation (via a receiver in the ear canal). This approach does not overcome some of the drawbacks of hearing aids, including occlusion effect, discomfort, feedback, and exacerbation of ear canal infections. These limitations have impacted the acceptance of hearing aids for rehabilitation of sensorineural and conductive hearing loss. Motivated by these considerations, we have proposed a bimodal intracochlear device capable of delivering both acoustic and electric stimulation via the scala tympani, minimizing some of the shortcomings of current acoustic components of hybrid electroacoustic cochlear implants. The constraints on delivery of acoustic stimulation directly to the perilymph (distinct from round and oval windows) and effects on residual hearing are poorly characterized (Lesinski et al., 2014; Schraven et al., 2015). In previous studies, we presented the characterization of a small, piezoelectric actuator with the desired response characteristics in vitro (Lee, Shen, Hume, & Cao, 2005; Luo, Cao, & Shen, 2013). In this study, we demonstrate

that this device can deliver acoustic stimuli directly to perilymph in the basal region of the guinea pig cochlea and generate auditory brainstem responses (ABRs) in vivo with latencies and growth functions comparable to acoustic stimulation in the ear canal. Our results suggest that this approach is promising to be effective and minimally traumatic. Further experiments will be necessary to evaluate the efficiency and safety of this modality in long-term auditory stimulation and its ability to be integrated with conventional cochlear implant arrays.

Materials and Methods

Fabrication of PZT Microactuator

The conceptual design, fabrication, and in vitro testing of an acoustic PZT microactuator for intracochlear applications has been documented in detail (Lee et al., 2005; Luo, Cao, et al., 2013). It is briefly summarized for reference. The physical dimensions and response parameters of the microactuator were initially chosen based on the size of the guinea pig (and human) scala tympani and vibrational properties of the stapes.

Figure 1 shows a schematic drawing of the PZT microactuator probe. The fabrication of the PZT actuator probes starts with the preparation of silicon wafers with oxide and nitride layers. Then the bottom electrode is deposited (Platinum over Titanium layers) and annealed. Next, a PZT layer is deposited via spin coating and sintered for the PZT to crystallize. Three rounds of deposition are needed to achieve the 1 μm thickness of the PZT layer. The top electrode (Gold over Chromium layers) is then deposited and patterned. Deep reactive-ion etching from the backside of the wafer forms the
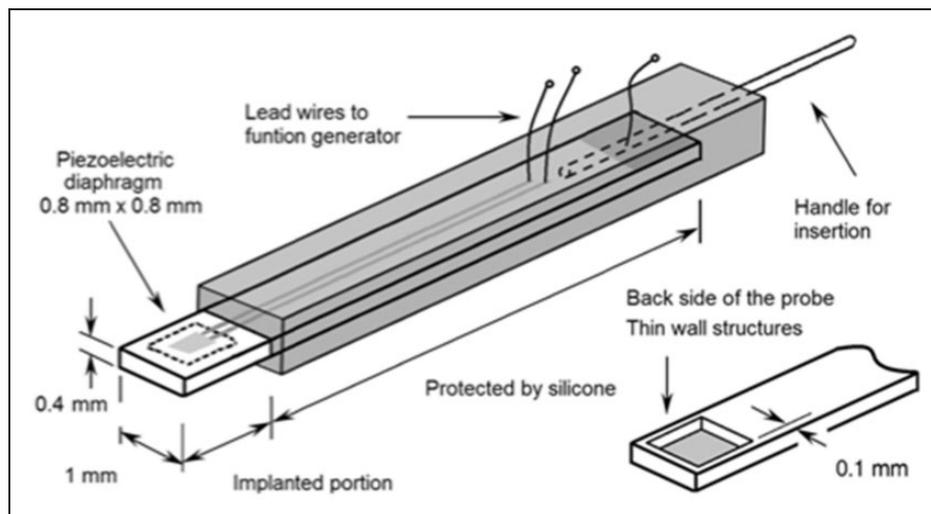
Figure 1. Conceptual design of a PZT thin-film microactuator probe.

diaphragm structure and simultaneously releases the PZT actuator probes from the wafer.

Figure 2 shows a photo of a completed fabricated probe. The probe is 1 mm wide, 0.4 mm thick, and roughly 20 mm long. At the tip of the probe, a very thin piezoelectric diaphragm spans an area of 0.8 mm by 0.8 mm. The diaphragm is 2 μm thick and consists of multiple layers, including, in sequence, a top electrode layer, a lead-zirconate-titanate (PZT) layer, a bottom electrode layer, and a silicon layer. The PZT and silicon layers are roughly the same thickness (1 μm each), and the electrode layers are significantly thinner. The top electrode layer is partitioned into two concentric components: a central electrode and an outer electrode. Each electrode can serve as a top electrode independently, or both can be driven simultaneously (with a phase shift) to enhance the actuation power of the PZT diaphragm. The relative size of the microactuator at the probe tip is shown in Figure 2(c).

When an alternating voltage is applied to the top and bottom electrodes, an electric field is developed in the PZT layer, extending and contracting the PZT. Since the diaphragm employs a bilayer configuration (i.e., PZT and silicon layers), the extension and contraction of the PZT layer will flex the diaphragm, emanating a pressure wave. Each fabricated probe is soldered with three electrode lead wires and tested for diaphragm displacement in vitro. Qualified probes are assembled into a custom-designed fixture for parylene packaging.

To avoid short circuiting, the probe in an aqueous environment, the entire PZT actuator probe is coated with a thin layer of parylene (0.25 μm thick). Parylene has previously been shown to be biocompatible in the cochlea (Mistry, Nolan, Saeed, Forge, & Taylor, 2014; Stover & Lenarz, 2009; Zeng, Rebscher, Harrison, Sun, & Feng, 2008). The proximal, rigid portion of the probe is embedded in silicone to facilitate fabrication and handling during surgery. The distal tip of the PZT actuator probe encompassing the diaphragm is inserted into the perilymph in the basal turn of the cochlea.

Characterization of PZT Microactuator In Vitro

Each PZT microactuator probe went through two tests to evaluate its performance prior to testing in vivo, a vibration test and an impedance test, which are described in the following subsections.

Vibration test. The purpose of this test is to identify the PZT actuator probe's bandwidth and sensitivity. A swept-sine voltage drives the PZT microactuator from 0 to 100 kHz while a laser Doppler vibrometer is used to measure the velocity at the center of the
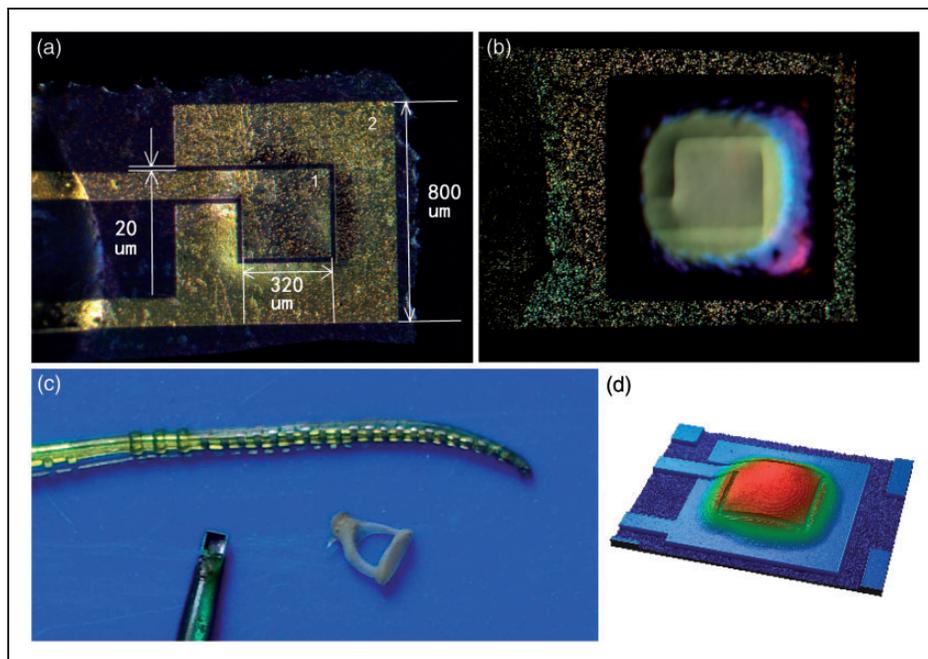
Figure 2. Photos of a fabricated PZT thin-film microactuator probe: (a) top view under an optical microscope revealing the top central (Actuator 1) and outer (Actuator 2) electrodes; (b) bottom view revealing the thin-wall structure around the square diaphragm, noting that the top central electrode can be identified; and (c) relative size of the microactuator at the tip of a probe compared with a conventional cochlear implant electrode (Cochlear Contour) and human stapes.

diaphragm. A spectrum analyzer processes the driving voltage and the measured velocity to obtain a frequency response function (FRF) of the PZT microactuator probe. For the measured FRF, we closely monitor two important properties.

The first is the natural frequency or resonant frequency. When the natural frequency is too high (e.g., above 100 kHz), the PZT diaphragm would tend to be too stiff, providing very little actuator displacement. When the natural frequency is too low (e.g., below 40 kHz), the added mass of the surrounding fluid in cochlea might reduce the natural frequency significantly affecting the bandwidth of the actuator (Luo, Cao, et al., 2013; Luo, Yang, Cao, & Shen, 2013). The probes used in the animal tests typically had first natural frequencies in air in a range between 50 and 90 kHz.

The second quantity of interest is the magnitude (or gain) of FRF below 5 kHz. This magnitude is in general a constant and reflects the displacement of the diaphragm. The larger the magnitude, the more power the actuator delivers (i.e., more sensitive). The probes used in the animal tests had diaphragm displacements in air ranging from 9.43 to 82.5 nm/V (Table 1).

The vibration test was also conducted in water and artificial perilymph to ensure that the parylene-encapsulated probes were functional in an aqueous environment (Foster & Luebke, 2002). In our previous work, we showed that the microactuator could function for a minimum of 54 hours in an aqueous environment. Surprisingly, the displacement actually increased in an aqueous environment relative to the dry configuration and the natural frequency shifts down to a narrow range around 16 kHz (Luo, Cao, et al., 2013; Luo, Yang, et al., 2013). This is hypothesized to result from intercalation of water molecules into pores in the PZT material (Luo, Cao, et al., 2013).

Impedance test. The purpose of the test is to measure the impedance of the PZT actuator probe in air and in artificial perilymph, thus evaluating effectiveness of the parylene coating in insulating the PZT probes from the surrounding perilymph electrically. The impedance analyzer sends out a sinusoidal voltage signal and the responding current is measured to obtain impedance of the PZT actuator probe as a function of the driving frequency. The measured impedance has a real part and an imaginary part, or equivalently a magnitude and a phase. The real part represents energy loss via resistance, and the imaginary part represents inductance or capacitance.

Ideally, PZT behaves like a capacitor in electrical circuit with a very tiny loss. Therefore, the measured impedance should have a phase angle very close to $-90°$. If the parylene coating does not insulate the PZT actuator probe properly, the electric current will leak from the top to bottom electrodes through the surrounding fluid causing additional resistance loss. As a result, the real part of the impedance will increase and the phase angle will drop significantly from $-90°$. For the PZT microactuator probes used in the animal tests, the phase angles of the measured impedance ranged from $-80°$ to $-90°$ and are summarized in Table 1.

Mechanically nonfunctional PZT microactuator probe. The ABR measured in the animal tests is theoretically a combined response of the mechanical actuation from the diaphragm deflection, as well as any electrical leakage (equivalent to an electrically evoked ABR) from the PZT microactuator circuitry into the perilymph.

Table 1. Actuator Response Properties.

Actuator		Presurgery		Postsurgery	
		Displacement in air (3 kHz)	Impedance in artificial perilymph	Displacement in air (3 kHz)	Impedance in artificial perilymph
Serial no.	Animal no.	Gain (nm/V)	Phase (°)	Gain (nm/V)	Phase (°)
27_C08	GP2	29.08	−89.01	broken	−86.65
27-C13	GP3	79.36	−88.94	82.5	−82.18
27-A06	GP4	39.36	−86.31	0 (malfunction)	−78.8
28-C04	GP4	9.43	Not tested	12.4	−88.91
27-A03	GP5	23.2	−89.33	No response	−89.58
27-C13	GP6	82.5	−82.18	84.2	−81.59
28-C10	GP8	30.3	−89.26	23.7	−89.15
27-C04	GP9	35.2	−89.41	Broken	Broken
27-C13*	GP9	0	−80.1	0	−79.8

Note. Displacement and impedance measurements of the inner microactuators (Actuator 1) were obtained before and after in vivo tests. 27-C13* was filled with epoxy before it was used with GP9.

This would be comparable to basal bipolar stimulation with a cochlear implant electrode. To evaluate the potential contribution of electrical leakage to the ABR, we developed a mechanically nonfunctional electrode as follows.

We filled the cavity of a PZT actuator probe with epoxy, so that the diaphragm would not deflect when voltage was applied. Prior to filling with epoxy, the response properties of the microactuator in vitro were comparable to the other probes. Because the epoxy was applied to the nonelectrode surface of the microactuator, any electrical leakage unshielded by the parylene should remain. By using such a probe, we were able to study effects of the electrical leakage in the absence of any mechanical stimulation.

After the animal tests were completed, we repeated the vibration and impedance tests of each microactuator to reevaluate the response properties. In some cases, this was not possible due to damage to the microactuator.

Surgical Procedure

Recordings were made in seven adult albino female Hartley guinea pigs (200 and 450 g) for different aspects of the testing. The University of Washington Institutional Animal Care and Use Committee approved all procedures.

Animals were anesthetized with Ketamine and Xylazine (50 mg/kg; 5 mg/kg). Subsequent anesthetic doses were given as needed at half-hour to 1-hour intervals using 1/2 to 1/3 the initial doses. The body temperature of each animal was maintained at 36°C to 38°C, using an isotherm heating pad. Small subdermal pin electrodes were placed at the vertex (positive), behind the ipsilateral mastoid (negative) and at the thigh (ground) for baseline ABR measurements (see later; Dobie & Berlin, 1979; Gardi & Berlin, 1981). An outline of the sequence and duration of the procedures is shown in Figure 3.

Using an operating microscope, a dorsal approach was used to expose the bulla and the underlying labyrinth. The bulla was opened by gently scraping with a scalpel to allow access to the round window niche. A low-speed diamond drill was then used to remove the bony overhangs surrounding the round window membrane. The Pre ABR was obtained at this time point. The round window membrane was then incised using a fine needle and the PZT microactuator probe inserted into the scala tympani for a distance of approximately 2 mm, until the diaphragm was submerged in perilymph. The device fit snuggly into the round window niche and there was minimal leakage of perilymph. The opening was not sealed to facilitate removal of the device after testing without damage. The PZT device was connected to lead wires that were used for stimulation.

Microactuator-evoked ABRs (A-ABR) were measured as outlined in the following. In some animals, an ABR using the ear canal coupler was repeated after removal of the device to assess mechanical/acoustic damage to the auditory pathway. To evaluate any electrical artifact from current leakage from the actuator, additional recordings were made 5 and 15 minutes after euthanasia.

Auditory Function Measurements

ABR measurements at 4, 8, 16, and 24 kHz pure tones were obtained prior to surgery and after each subsequent manipulation. The ABR stimulus generation, calibration, data acquisition, and storage system was controlled using the Eaton Peabody Laboratory Cochlear Function Test Suite and ABR Wave Analyzer software (EPL-CFTS, 2015; Kujawa & Liberman, 2006).

Acoustic stimuli. Acoustic stimuli were generated digitally, attenuated using programmable attenuators, and delivered via electrostatic speakers (RP-2, PA-5, ED-1, and EC-1; Tucker-Davis Technologies, Alachua, FL, USA)
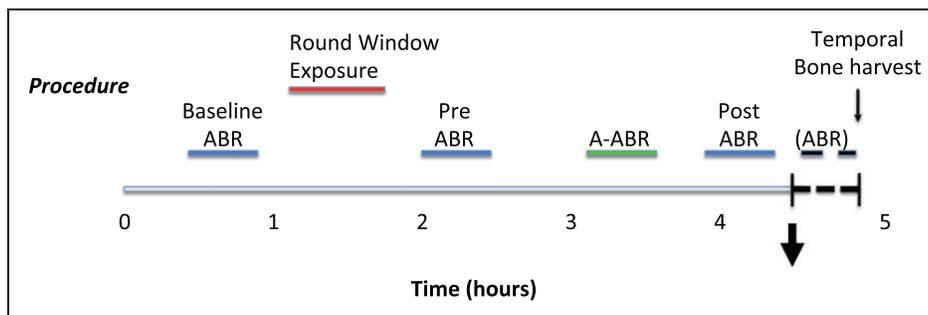
Figure 3. Timeline of procedures. The approximate duration and sequence of each procedure is indicated by the solid bar. ABR = auditory brainstem response using ear canal coupler; A-ABR = auditory brainstem response using microactuator in scala tympani. Heavy downward arrow indicates time of euthanasia.

connected to the ear by a 0.3-inch long metal coupler tube inserted into the external canal. The stimuli (5 ms, 0.5 ms rise/fall, 4 ms plateau) were presented at a rate of 25/s. Prior to the ABR recording, the speakers were calibrated across the frequency range using a probe tube microphone (Type 4133; Bruel & Kjaer, Denmark).

Microactuator stimuli. The microactuator stimuli were generated using the same software as the acoustic stimuli (EPL-CFTS, 2015; Kujawa & Liberman, 2006). Instead of relying on the decibel level indicated by the program, an oscilloscope was used to determine the voltage values produced by the program. This calibrated signal was applied across the electrode of the microactuator to produce an out-of-plane motion via the piezoelectric effect. By increasing the magnitude of the applied signal, the magnitude of the diaphragm's motion was correspondingly increased. By varying the signal sent to the microactuator, auditory thresholds were visually determined for each frequency tested.

Recording. ABR signals were amplified 10,000 times using a biological amplifier (Grass CP-511) and filtered (0.1 - to 3 kHz). The signal was digitized and 350 trials were averaged at each frequency. Stimuli were incremented in systematic 5-dB steps from below threshold to 80 dB. Artifact rejection was set to 15 µV peak to peak. The threshold was defined as the lowest level at which Wave I of the ABR could be clearly detected by visual inspection.

Data were statistically analyzed using GraphPad Prism 6.0 (GraphPad Software, Inc., CA, USA). Values of *p* below.05 were considered significant.

Histological Analysis

Tissue preparation. Guinea pigs were sacrificed by Euthasol (pentobarbital/phenytoin) injection after measurements were completed. After removal of the bulla, the stapes was lifted from the oval window and small openings were made in the apical turn. Cold 4% paraformaldehyde in 0.1 M phosphate-buffered saline (PBS), pH 7.4, was perfused slowly through the cochlea and the temporal bones fixed for 2 hours at room temperature. Following fixation, the temporal bones were washed 3 times (10 minutes each) in PBS (pH 7.4). The tissue was prepared as whole-mount preparations (Hume, Bratt, & Oesterle, 2007; Oesterle, Sarthy, & Rubel, 1990; Tong et al., 2015). For the former, segments (half turns) of the organ of Corti were carefully dissected free from the cochlea, the lateral wall was pulled off or trimmed down, and the tectorial membrane lifted free with fine forceps.

Immunofluorescent labeling. A rabbit myosin 6 polyclonal antibody (Proteus Biosciences, Ramona, CA, Cat.

No. 25-6791, 1:500) was used to label hair cells. The specificity of this antibody has been verified in previous published work (Ferri et al., 2004; Hume et al., 2007; Tong et al., 2015). To visualize hair cell stereociliary bundles, cuticular plates, and supporting cell profiles, filamentous actin was labeled with phalloidin directly conjugated to a fluorophore (Alexa 488, Invitrogen Corp., Eugene, OR, Cat. No. A12381, 1:50 dilution).

The tissue was permeabilized for 60 minutes with 0.1% Triton X-100/BSA in PBS. To prevent nonspecific binding of the primary antibody, tissues were then incubated for 60 minutes in a blocking solution consisting of 5% normal serum/0.03% saponin/0.1% Triton X-100 in PBS. Primary antibody incubations were performed overnight at 4°C in blocking solution (Hume et al., 2007). Fluorescent-conjugated secondary antibodies (Alexa 568, Invitrogen/Molecular Probes) were used at a dilution of 1:200 in the same buffer for 4 hours (at room temperature). Sections were washed after each antibody was incubated (3 times for 10–15 minutes each) in 0.1% Tween 20 in PBS. Conjugated phalloidin was incubated with tissues for 60 minutes at room temperature, washed in PBS (3×10 minutes). After counterstaining nuclei with DAPI (Cat. No. D9542, Sigma-Aldrich, 1 µg/ml), specimens were mounted in Vectashield (Vector Laboratories), coverslipped, and examined with confocal fluorescence microscopy.

Microscopic imaging. Whole-mount organ of Corti preparations were viewed with an Olympus FV-1000 laser scanning confocal microscope. Fluoview version 1.4a acquisition software was used. Files were imported into ImageJ 1.42a (NIH) and Adobe Photoshop CS version (Adobe, Seattle WA) for processing and analysis. Histogram stretch was performed on each image with Photoshop to increase contrast of immunofluorescence against background. Control and experimental images were treated the same in all instances.

Results

Our goal is to develop a microactuator for direct acoustic stimulation of the perilymph, bypassing the middle ear. We envision incorporating the actuator into a hybrid cochlear implant electrode array that also contains electrodes for electrical stimulation. In our previous work, we described the design, preliminary fabrication, and in vitro response properties of a microactuator designed for intracochlear applications (Lee et al., 2005; Luo, Cao, et al., 2013). This device demonstrated the appropriate response properties for acoustic stimulation through the useful auditory frequency range for human hearing (20–20,000 Hz), and was functional for 54 hours in an aqueous environment (Luo, Cao, et al., 2013).
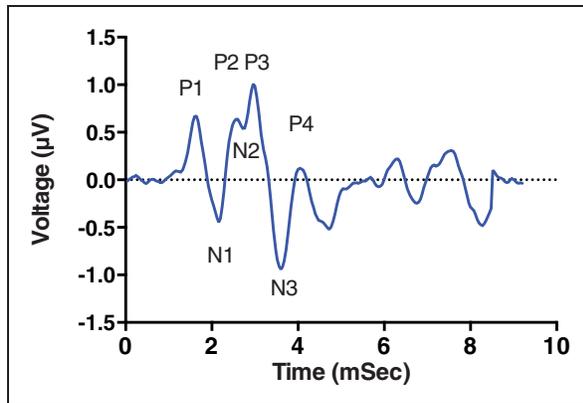
Figure 4. ABR waveform morphology. A typical waveform (GP6, 16 kHz, 80 dB SPL) obtained for auditory stimulation via an ear canal coupler in the guinea pig. Peaks (P) and troughs (N) are indicated.

For the present studies, a number of microactuator probes were fabricated and tested in vitro and in vivo in an adult guinea pig model. The displacement and impedance characteristics of the probes used in animal experiments are noted in Table 1.

ABR Testing

We measured baseline auditory evoked responses in a closed field system using an ear canal microphone and calibrated tone pips delivered to the right ear. Figure 4 shows typical positive (P) and negative peaks (N) noted in ABR waveforms as described previously in guinea pig (shown for GP6, 16 kHz, 80 dB SPL). The VIII nerve generates P1-N1, while P2 originates in the cochlear nucleus, and P3/N3 is attributed to the superior olivary complex and medial nucleus of the trapezoid body. The latencies of waves P1-P4 were comparable to those described in the literature (Brown & Patuzzi, 2010; Dehmel, Eisinger, & Shore, 2012; Dobie & Berlin, 1979; Gardi & Berlin, 1981).

Figure 5 shows suprathreshold responses from two individual animals (GP6, Column A and GP8, Column B) in response to stimuli at 4, 8, 16, and 24 kHz. A complete set of ABR data was obtained for three animals with three different actuators across the range of frequencies (GP6, 8, 9; see also Table 1 and Figure 6). More limited ABR data were obtained from four additional animals (GP2, 3, 4, and 5). At 4 and 8 kHz, P2-N2-P3 often formed a single complex and a consistently higher noise floor was noted at 4 kHz, compared with higher frequencies.

A baseline ABR was obtained after anesthesia using an ear canal coupler (not shown). We used a standard dorsal postauricular approach to expose the bulla. The bulla was opened and the round window niche exposed.

The bone overlying the niche was gently enlarged with a diamond drill to expose the round window. A repeat ABR with the ear canal coupler showed comparable evoked responses at each frequency (Pre ABR).

Microactuator ABR Testing

The round window membrane was opened with a needle and the probe tip advanced into the basal scala tympani until the microactuator was completely immersed in perilymph (approximately 1.5–2 mm). The body of the electrode probe was stabilized in the bulla so that the microactuator was roughly parallel to the basilar membrane. Because there was minimal leakage of perilymph around the actuator tip, we did not place any additional sealant. In these pilot studies, we were also concerned that fixation would prevent atraumatic removal of the actuator for postsurgical ear canal coupler ABR testing. The EPL-CFTS stimulation software was used to deliver stimuli to the microactuator across the same range of frequencies and responses that were tested with the ear canal coupler. Because we cannot measure the diaphragm displacement or sound pressure level in situ in the scala tympani, a *true* decibel presentation level cannot be determined. The starting stimulation voltage was based on levels predicted to be below threshold by measuring the voltage output to the ear canal coupler at plateau (approximately 10 V) and the corresponding voltage decremented by 65 dB to account for the approximate dynamic range. In cases where a clear waveform was noted, we decreased the level further. Stimuli were incremented in sequential 5 dB steps until a clear response was obtained.

Suprathreshold responses at 4, 8, 16, and 24 kHz are shown in Figure 5. The individual tracings that are shown were chosen to approximately match the amplitudes of Wave I between paradigms. We deliberately did not seek to maximize evoked response amplitudes to avoid intracochlear damage during our initial testing. In some animals, both the inner (Actuator 1) and outer (Actuator 2) concentric microactuator electrodes were tested at each frequency (Figure 5(a), GP6). Responses were generally more robust from Actuator 1.

ABR Responses to Microactuator Are Comparable to Ear Canal Stimulation

Wave I peak latencies and interpeak latencies from Wave I to Wave III were measured for both auditory (ABR, I: 1.86 ± 0.16 μs; I–III: 1.56 ± 0.04 μs at 16 kHz, GP8) and microactuator (A-ABR, I: 1.92 ± 0.21 μs; I–III 1.9 ± 0.10 μs at 16 kHz, GP8) stimulation and are comparable to other published studies on ABR in guinea pig. This contrasts to shortened latencies when an electrical stimulus is delivered to the perilymph in an E-ABR
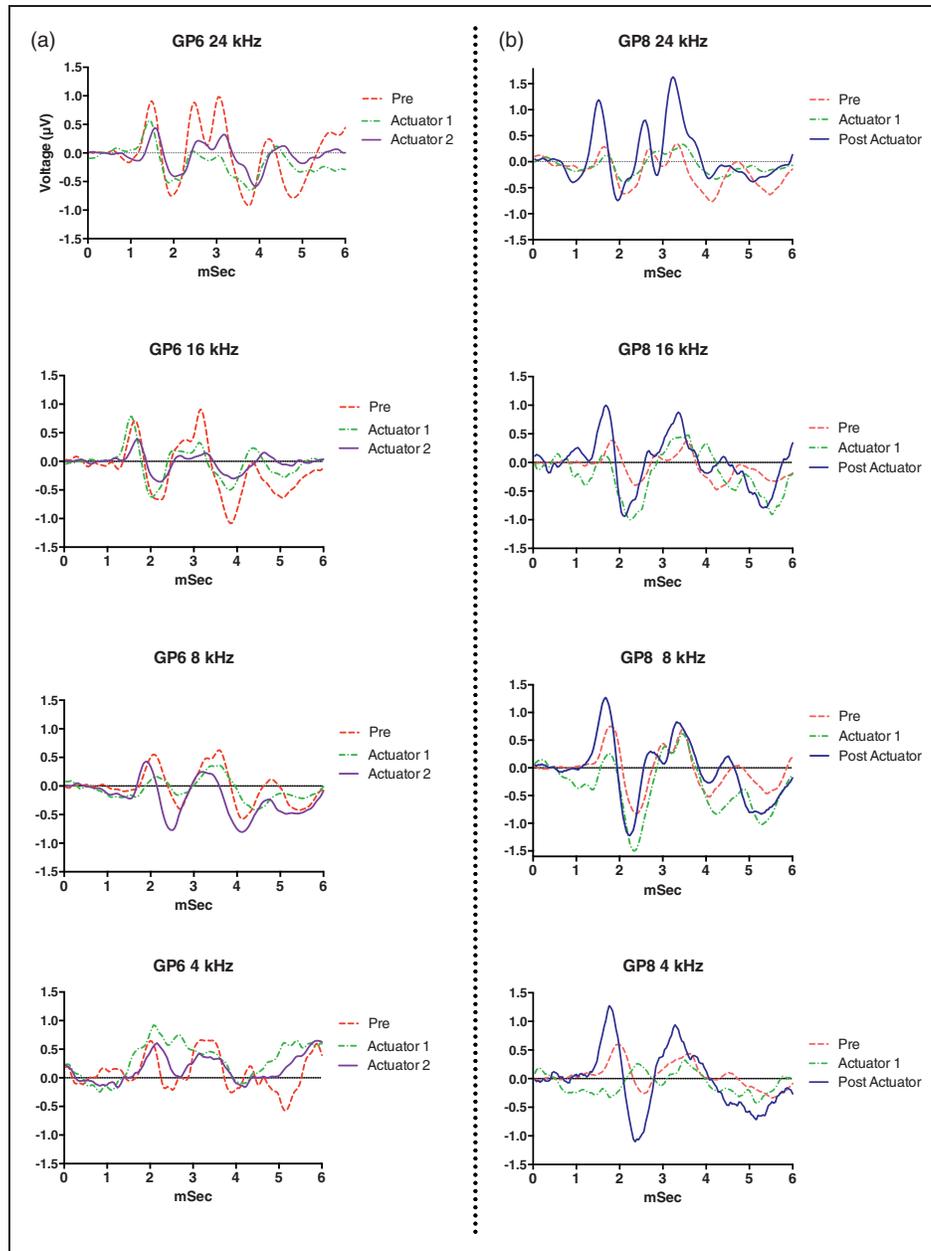
Figure 5. Representative ABR data. Waveforms obtained with an ear canal coupler after surgical exposure of the round window (Pre) and with the acoustic microactuator for two animals at 4, 8, 16, and 24 kHz (GP6, a; GP8, b). In (a), the inner (Actuator 1) or outer (Actuator 2) electrodes were tested independently. In (b), ABR responses to the ear canal coupler were also measuredafter removal of the microactuator (Post Actuator).

and suggests that the microactuator device is stimulating responses via a mechanical rather than an electrical process (leakage) (Marsh, Yamane, & Potsic, 1981; Noh et al., 2007; Yamane, Marsh, & Potsic, 1981).

The growth response functions of Wave I (P1 + N1) for stimulation via either the ear canal coupler or a microactuator are shown in Figure 6. The slopes of the growth functions obtained with the ear canal coupler are

similar for three individual guinea pigs (Figure 6(a) and (b)), while slopes with the actuators in the same animals are more variable (Figure 6(c)). Because the specific actuator and placement in the scala tympani differ in each guinea pig, we cannot directly compare slopes between actuators. Comparison of the gains for individual actuators suggests that this may be a major contributor. For example, actuator 27-C13, in GP6, has highest gain and
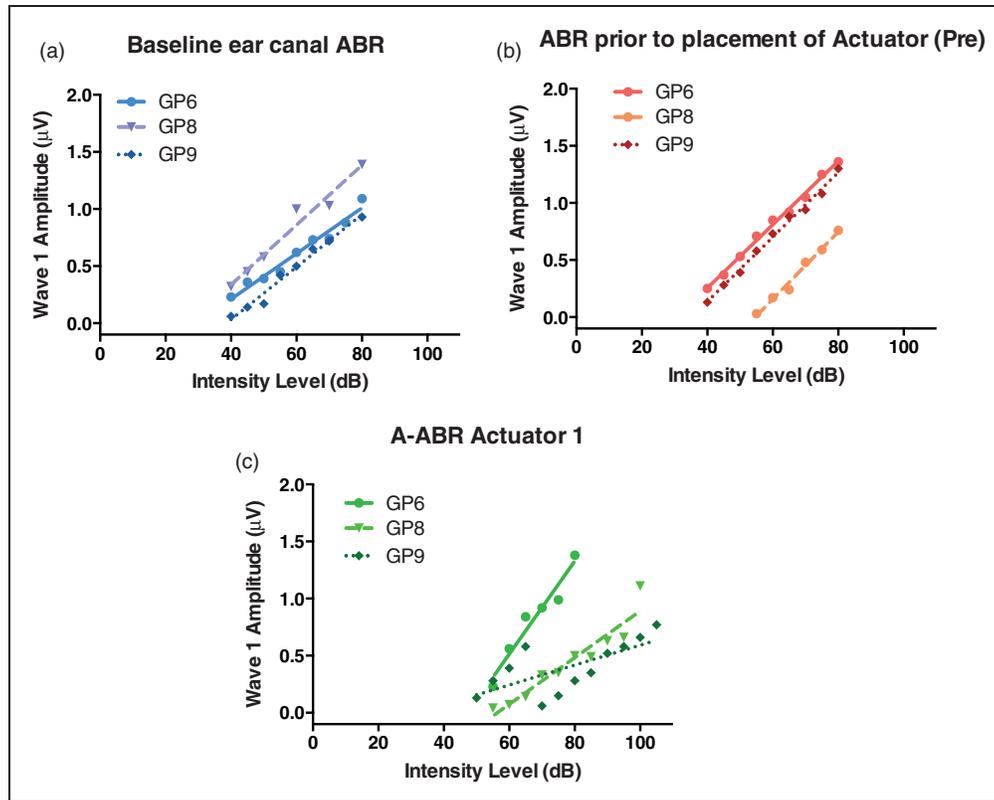
Figure 6. Amplitude growth functions (Wave I, P1 + N1). Plots are shown for three animals for stimulation via an ear canal coupler at baseline (a), after surgical exposure of the round window (b), and in response to the acoustic microactuator (c). (Data shown for 16 kHz.)

steepest slope (see also Table 1). Similarly, the abrupt change in Wave I amplitude between 65 and 70 dB noted in GP9 (Figure 6(c)) could relate to a change in actuator properties during testing, or positioning. Further replication will clarify these variables.

Effects of Surgery and Microactuator Stimulation on Residual Hearing

Preservation of residual hearing is critical for the goal of the intracochlear microactuator. Due to physical constraints on positioning the microactuator and the ear canal probe at the same time, we were unable to measure an acoustic ABR with the microactuator in place with our current device. As one measure of trauma caused by the surgical procedure and microactuator stimulation, in one animal we repeated ABR testing using the ear canal coupler after removal of the microactuator (Figure 5(b), Post Actuator). This verified that auditory responses to ear canal delivered stimuli were at least partially preserved after removal of the microactuator with typical waveforms. Because the round window remained unsealed after removal of the microactuator from the round window and coupler positioning is also variable, thresholds and waveforms are not superimposable on the

baseline ear canal ABR, but Waves I to III are easily identifiable.

Controls for Current Leakage

In early trials of stimulation with some of the microactuator probes, there was a discharge pattern that did not correspond with expected ABR waveform. This became more dramatic at higher stimulation voltages and was never seen with the ear canal microphone. This suggested that a component of the stimulation via the microactuator might arise directly from electrical leak from the device. To assess this concern directly, we tested an electrode filled with epoxy to render it mechanically nonfunctional but preserve any current leakage contribution. As shown in Figure 7(a), the filled device did not generate a typical ABR waveform at comparable maximal stimulus levels (up to 10 V). These studies were consistent with the microactuator probe leading to an auditory response via perilymph rather than through direct electrical leakage.

We also repeated the stimulation using the microactuator 15 minutes after the animal was sacrificed to ensure that an active auditory process was responsible for the responses noted (Figure 7(b)).
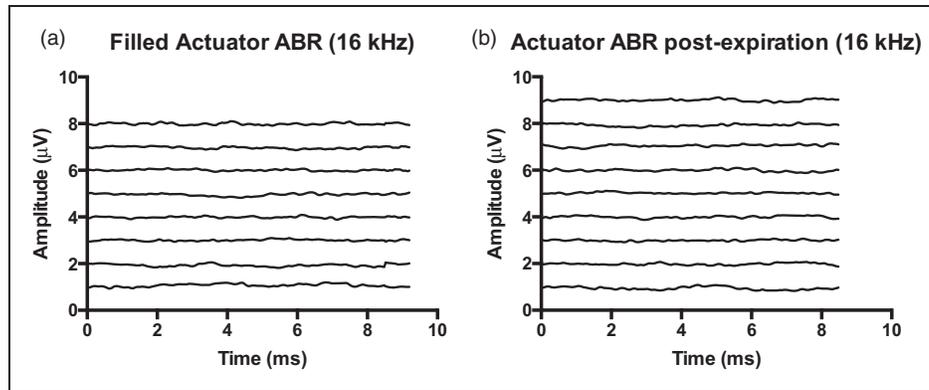
Figure 7. Controls for specificity of microactuator responses. (a) An epoxy-filled microactuator does not stimulate auditory responses. (b) Comparable auditory responses are not obtained from euthanized animals. (Data shown for 16 kHz.)
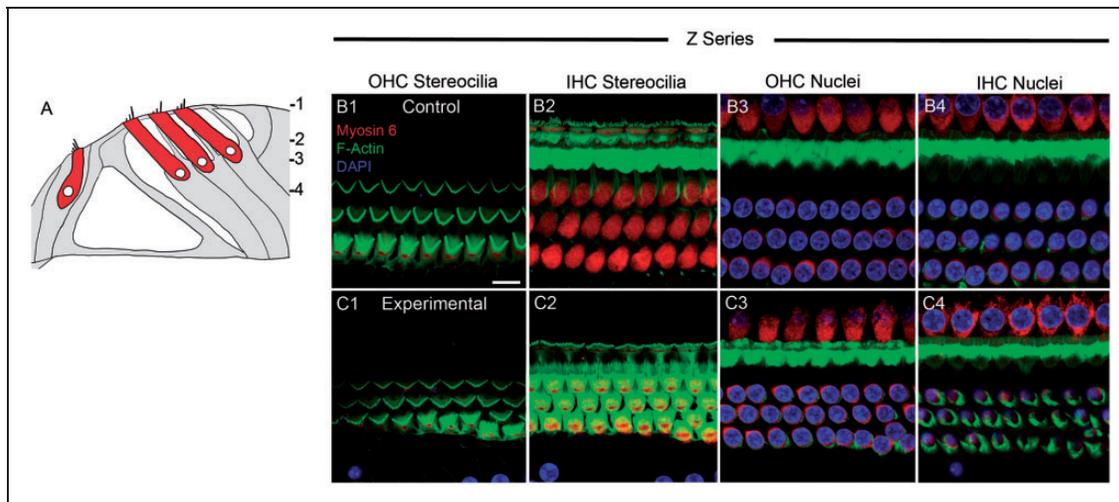
Figure 8. Inner and outer hair cells remain throughout the cochlea after microactuator stimulation. Horizontal confocal slices taken from one field of a control (B1–B4) and microactuator-stimulated (C1–C4) basal cochlea at successive depths in the epithelium. (a) Schematized transverse section of the organ of Corti illustrating the positions of confocal slices shown in B1–B4 and C1–C4. (b, c) Whole-mounted tissue was immunolabeled with myosin 6 antibody (red) that specifically labels hair cells and phalloidin (green) that labels F-Actin, including actin in hair cell stereocilia. The nuclear counterstain DAPI (blue) labeled all nuclei. (c) Stereocilia bundles remain in the microactuator-stimulated ear and hair cell nuclei are normal in morphology. Scale bar = 10 μm in B1 (applies to B1–B4 and C1–C4).

Histological Analysis of Damage

We evaluated potential trauma caused by the surgical exposure and microactuator stimulation using histology. After a full sequence of testing, the temporal bone was harvested from both ears of several animals and processed for analysis of gross trauma, stereociliary damage, nuclear damage, and loss of hair cells by confocal microscopy using markers for hair cells, nuclei, and stereocilia. On the basis of the proximity to the surgical site, we expected that the basal cochlea would suffer the most damage. This region is shown in a series of confocal planes through the organ of Corti in Figure 8. We did not identify any differential loss or damage to inner or outer hair cells between the stimulated ear and the control, contralateral ear. In contrast to some models of noise damage, we did not identify any sign of stereociliary fusion or loss of bundles in inner or outer hair cells with phalloidin labeling (Figure 8, B1, C1). Nuclei also appeared normal (Figure 8, B3/4, C3/4). We occasionally noted subtle changes in the intensity of myosin VI labeling in inner hair cells that were not seen in the control contralateral ear (not shown). Because sound and surgical trauma were both delivered at ear level, the significance of these changes is unknown and they could be related to surgical exposure, microactuator placement

or potentially to the sound stimulus itself. In these short-term studies, we did not evaluate the morphology of afferent terminals on hair cells (Kujawa & Liberman, 2009; Liu et al., 2012; Shi et al., 2013).

Discussion

There are a number of barriers to acceptance of ear canal level hearing aids, including discomfort, feedback, and recurrent inflammation. We describe the initial in vivo characterization of an intracochlear acoustic microactuator that addresses some of these limitations by directly stimulating the perilymph. We show that the microactuator in the guinea pig basal turn scala tympani is able to stimulate ABR responses across a range of frequencies from 4 to 24 kHz without deafening or obvious signs of cochlear trauma. ABR amplitudes that are comparable to stimulation via the ear canal can be readily achieved using the microactuator in the scala tympani. In individuals with middle ear or ossicular deficits, there may also be biomechanical advantage of direct delivery of acoustic stimuli to the perilymph versus the ossicular chain or tympanic membrane. We envision this device could also function as a component of an integrated bimodal acoustic-electric electrode array in individuals who are candidates for electroacoustic stimulation. The current work is a proof of concept and further experiments will be necessary to evaluate the efficiency and safety of this modality in long-term auditory stimulation and its ability to be integrated with conventional cochlear implant arrays.

The majority of candidates for EAS have preserved hearing in the low frequencies (<1000 Hz). Perhaps surprisingly, despite positioning in the perilymph of the scala tympani, cochlear implant electrodes do not necessarily dramatically compromise acoustic hearing (Choi & Oghalai, 2005; Chole, Hullar, & Potts, 2014; Greene et al., 2015; Huber, Hoon, Sharouz, Daniel, & Albrecht, 2010). Sound transmission through cochlear fluids appears to follow multiple pathways that remain somewhat controversial (Lee et al., 2015; Lee, Seong, Lee, Lee, & Cho, 2014; Nakajima, Merchant, & Rosowski, 2010; Ni, Elliott, Ayat, & Teal, 2014; Ren, He, & Gillespie, 2011). The role of a compressive fluid wave versus basilar membrane deflection and carrier wave is unclear and may differ across frequencies. Based on the vector of insertion in our experiments, the microactuator PZT diaphragm is positioned roughly parallel to the basilar membrane and the rigid surrounding silicon framework is stabilized at the round window. This may facilitate initiation of a basilar membrane carrier wave.

Some models of stapes dynamics suggest that low-frequency signals may require volume displacement for auditory stimulation. Because the actuator diaphragm is completely immersed in perilymph, it should not cause any net fluid displacement, and there may be a small amount of leakage around the device. The reported average stapes dimensions in the guinea pig are $1.44 \pm 0.034 \times 0.66 \pm 0.029$ mm, with an effective area of 0.79 ± 0.039 mm^2 (Sim, Röösli, Chatzimichalis, Eiber, & Huber, 2013). However, we find that the actuator diaphragm measuring 0.8 mm × 0.8 mm is effective at stimulating responses across a range of frequencies.

We did find that responses were less robust at 4 kHz than at higher frequencies. 4 kHz is at the lower range of guinea pig hearing, and in our studies even with an ear canal coupler, responses at 4 kHz were less robust, with a higher noise floor (Heffner & Heffner, 2007). Alternative primate models with a range of hearing more comparable to humans may be necessary to assess the importance of fluid volume displacement for adequate response in vivo. With further development of smaller concentric electrodes and chronic implantation, we may be able to directly test the effects of the diaphragm orientation for delivery of acoustic stimuli and facilitate the analysis of mechanisms of intracochlear sound transmission.

Studies of EAS have shown improvements in hearing preservation, speech understanding, and spatial awareness (Talbot & Hartley, 2008; Turner & Gantz, 2012). Despite these encouraging results, about a third of patients eventually lose hearing in the implanted ear (Barbara et al., 2003; Gstoettner et al., 2006; Woodson et al., 2010). Although our acute experiments do not show obvious damage, it is unknown if an acoustic actuator would accelerate hearing loss relative to a conventional cochlear implant electrode array. The limited studies of temporal bone histology of cochlear implant recipients with initially preserved hearing show that scar tissue may form in the basal cochlea (Nadol et al., 2001; Nadol et al., 2015; O'Leary et al., 2013). Longer follow-up of hybrid cochlear implant recipients suggests that previously stable thresholds may deteriorate over a more extended time frame even when initially preserved, suggesting that not all deterioration is related to inflammation (Kopelovich et al., 2015; Reiss et al., 2015).

More recent studies have shown that maximal ABR Wave I amplitudes may decline following high-level sound exposure even though Wave I thresholds remain similar. This correlates with a decline in afferent innervation of inner hair cells that was not assessed in our study (Kujawa & Liberman, 2009; Liu et al., 2012; Shi et al., 2013). If appropriately calibrated, it is unknown whether an intracochlear microactuator would accelerate the loss of residual hearing more than continued auditory stimulation via an ear canal hearing aid or the trauma related to cochlear implantation. We plan to address these concerns in longer term in vivo experiments with a chronic microactuator in place.

Lesinski et al. (2014) have recently described a titanium microactuator to be implanted through the lateral wall of cochlea into the scala tympani that has some similarities to our PZT device (OtoKinetics.com). While their device was nonfunctional, it did not cause any significant detriment to hearing in a chronically implanted cat model. The efficiency of this titanium device in delivering auditory stimulation across frequencies in vivo has not yet been demonstrated. Schraven et al. (2015) have shown that the floating mass transducer (FMT) of the Vibrant Soundbridge (MED-EL) can be directly coupled to an in situ cochlear implant electrode array and generate stapes displacement in a cadaveric temporal bone study. This configuration differs substantially from our device because the FMT vibration is transmitted along the electrode itself into the scala tympani. The potential effects of an FMT-electrode on perilymph homeostasis, intracochlear trauma, residual hearing, and frequency response properties are not yet well characterized for comparison.

PZT is a perovskite structured material used extensively used in piezoelectric devices because of its powerful electromechanical conversion. During their life cycle, PZT piezoelectrics may leach into the local environment. Our current actuator is coated in parylene, a biocompatible material that may not be suitable for long-term in vivo use (Esquivel-Gaon et al., 2015). Little is known about PZT toxicity and interactions with biomolecules (Esquivel-Gaon et al., 2015). Strategies to alleviate this problem include packaging the PZT actuator in a leak-resistant enclosure or using an alternate, lead-free piezoelectric material. We are optimistic that in the future lead-free substitutes will become available that provide all the piezoelectric attributes without leaching toxic material.

Declaration of Conflicting Interests

The authors declared no potential conflicts of interest with respect to the research, authorship, and/or publication of this article.

References

Barbara, M., Mattioni, A., Monini, S., Chiappini, I., Ronchetti, F., Ballantyne, D.,…,Filipo, R. (2003). Delayed loss of residual hearing in Clarion cochlear implant users. *Journal of Laryngology & Otology*, *117*(11), 850–853. doi:10.1258/002221503322542836

Blackwell, D. L., Lucas, J. W., & Clarke, T. C. (2014). Summary health statistics for U.S. adults: National health interview survey, 2012. *Vital Health Stat 10*, *260*, 1–161. Retrieved from http://www.ncbi.nlm.nih.gov/entrez/query.fcgi?cmd=Retrieve&db=PubMed&dopt=Citation&list_uids=24819891

Brown, D. J., & Patuzzi, R. B. (2010). Evidence that the compound action potential (CAP) from the auditory nerve is a stationary potential generated across dura mater. *Hearing Research*, *267*(1–2), 12–26. doi:10.1016/j.heares.2010.03.091

Choi, C. H., & Oghalai, J. S. (2005). Predicting the effect of post-implant cochlear fibrosis on residual hearing. *Hearing Research*, *205*(1–2), 193–200. doi:10.1016/j.heares.2005.03.018

Chole, R. A., Hullar, T. E., & Potts, L. G. (2014). Conductive component after cochlear implantation in patients with residual hearing conservation. *American Journal of Audiology*, *23*(4), 359–364. doi:10.1044/2014_AJA-14-0018

Dehmel, S., Eisinger, D., & Shore, S. E. (2012). Gap prepulse inhibition and auditory brainstem-evoked potentials as objective measures for tinnitus in guinea pigs. *Frontiers in Systems Neuroscience*, *6*, 42. doi:10.3389/fnsys.2012.00042

Dobie, R. A., & Berlin, C. I. (1979). Binaural interaction in brainstem-evoked responses. *Archives of Otolaryngology*, *105*(7), 391–398. Retrieved from http://www.ncbi.nlm.nih.gov/entrez/query.fcgi?cmd=Retrieve&db=PubMed&dopt=Citation&list_uids=454297

EPL-CFTS. (2015). *Eaton-peabody laboratories cochlear function test suite*Retrieved from http://www.masseyeandear.org/research/otolaryngology/investigators/laboratories/eaton-peabody-laboratories/epl-engineering-resources/epl-cochlear-function-test-suite

Esquivel-Gaon, M., Anguissola, S., Garry, D., Gallegos-Melgar, A. D. C., Saldaña, J. M., Dawson, K. A.,…,Del Razo, L. M. (2015). Bismuth-based nanoparticles as the environmentally friendly replacement for lead-based piezoelectrics. *RSC Advances*, *5*(35), 27295–27304. Retrieved from http://www.researchgate.net/profile/Luz_Maria_Del_Razo/publication/273685785_Bismuth-based_nanoparticles_as_the_environmentally_friendly_replacement_for_lead-based_piezoelectrics_/links/550863970cf2d7a28128f3ff.pdf

Ferri, A. L., Cavallaro, M., Braida, D., Di Cristofano, A., Canta, A., Vezzani, A.,…,Nicolis, S. K. (2004). Sox2 deficiency causes neurodegeneration and impaired neurogenesis in the adult mouse brain. *Development*, *131*(15), 3805–3819. doi:10.1242/dev.01204

Foster, P. K., & Luebke, A. E. (2002). A model for perilymphatic fistula induced hearing loss in the guinea pig cochlea. *Hearing Research*, *167*(1–2), 175–179. Retrieved from http://www.ncbi.nlm.nih.gov/entrez/query.fcgi?cmd=Retrieve&db=PubMed&dopt=Citation&list_uids=12117540

Gantz, B. J., & Turner, C. W. (2003). Combining acoustic and electrical hearing. *Laryngoscope*, *113*(10), 1726–1730. Retrieved from http://www.ncbi.nlm.nih.gov/entrez/query.fcgi?cmd=Retrieve&db=PubMed&dopt=Citation&list_uids=14520097

Gardi, J. N., & Berlin, C. I. (1981). Binaural interaction components. Their possible origins in guinea pig auditory brainstem response. *Archives of Otolaryngology*, *107*(3), 164–168. Retrieved from http://www.ncbi.nlm.nih.gov/entrez/query.fcgi?cmd=Retrieve&db=PubMed&dopt=Citation&list_uids=7469904

Greene, N. T., Mattingly, J. K., Jenkins, H. A., Tollin, D. J., Easter, J. R.Cass, S. P. (2015). Cochlear Implant Electrode Effect on Sound Energy Transfer Within the Cochlea During Acoustic Stimulation. *Otology & Neurotology*, *36*(9), 1554–1561. doi:10.1097/MAO.0000000000000838

Gstoettner, W., Kiefer, J., Baumgartner, W. D., Pok, S., Peters, S.Adunka, O. (2004). Hearing preservation in cochlear implantation for electric acoustic stimulation. *Acta Oto-Laryngologica*, *124*(4), 348–352. Retrieved from http://www.ncbi.nlm.nih.gov/entrez/query.fcgi?cmd=Retrieve&db=PubMed&dopt=Citation&list_uids=15224851

Gstoettner, W. K., Helbig, S., Maier, N., Kiefer, J., Radeloff, A.Adunka, O. F. (2006). Ipsilateral electric acoustic stimulation of the auditory system: Results of long-term hearing preservation. *Audiology and Neurotology*, *11*(Suppl 1): 49–56. doi:10.1159/000095614

Heffner, H. E., & Heffner, R. S. (2007). Hearing ranges of laboratory animals. *Journal of the American Association for Laboratory Animal Science*, *46*(1), 20–22. Retrieved from http://www.ncbi.nlm.nih.gov/entrez/query.fcgi?cmd=Retrieve&db=PubMed&dopt=Citation&list_uids=17203911

Huber, A. M., Hoon, S. J., Sharouz, B., Daniel, B., & Albrecht, E. (2010). The influence of a cochlear implant electrode on the mechanical function of the inner ear. *Otology & Neurotology*, *31*(3), 512–518. doi:10.1097/MAO.0b013e3181ca372b.

Hume, C. R., Bratt, D. L., & Oesterle, E. C. (2007). Expression of LHX3 and SOX2 during mouse inner ear development. *Gene Expression Patterns*, *7*(7), 798–807. Retrieved from http://www.ncbi.nlm.nih.gov/entrez/query.fcgi?cmd=Retrieve&db=PubMed&dopt=Citation&list_uids=17604700

Irving, S., Gillespie, L., Richardson, R., Rowe, D., Fallon, J. B.Wise, A. K. (2014). Electroacoustic stimulation: Now and into the future. *BioMed Research International*, *2014*, 350504doi:10.1155/2014/350504

Kochkin, S. (2010). MarkeTrak VIII: Consumer satisfaction with hearing aids is slowly increasing. *The Hearing Journal*, *63*(1), 19–20. Retrieved from http://journals.lww.com/thehearingjournal/Fulltext/2010/01000/MarkeTrak_VIII__Consumer_satisfaction_with_hearing.4.asp

Kopelovich, J. C., Reiss, L. A., Etler, C. P., Xu, L., Bertroche, J. T., Gantz, B. J.,...,Hansen, M. R. (2015). Hearing loss after activation of hearing preservation cochlear implants might be related to afferent cochlear innervation injury. *Otology & Neurotology*, *36*(6), 1035–1044. doi:10.1097/MAO.0000000000000754

Kujawa, S. G., & Liberman, M. C. (2006). Acceleration of age-related hearing loss by early noise exposure: Evidence of a misspent youth. *Journal of Neuroscience*, *26*(7), 2115–2123. Retrieved from http://www.ncbi.nlm.nih.gov/entrez/query.fcgi?cmd=Retrieve&db=PubMed&dopt=Citation&list_uids=16481444

Kujawa, S. G., & Liberman, M. C. (2009). Adding insult to injury: Cochlear nerve degeneration after "temporary" noise-induced hearing loss. *Journal of Neuroscience*, *29*(45), 14077–14085. doi:10.1523/JNEUROSCI.2845-09.2009

Lee, H. Y., Raphael, P. D., Park, J., Ellerbee, A. K., Applegate, B. E.Oghalai, J. S. (2015). Noninvasive in vivo imaging reveals differences between tectorial membrane and basilar membrane traveling waves in the mouse cochlea. *Proceedings of the National Academy of Sciences of the USA*, *112*(10), 3128–3133. doi:10.1073/pnas.1500038112

Lee, J., Seong, K., Lee, S. H., Lee, K. Y., & Cho, J. H. (2014). Comparison of auditory responses determined by acoustic stimulation and by mechanical round window stimulation at equivalent stapes velocities. *Hearing Research*, *314*, 65–71. doi:10.1016/j.heares.2014.04.003

Lee, C. C., Shen, I., Hume, C., & Cao, G. (2005). a feasibility study of PZT thin-film microactuators for hybrid cochlear implants. *Conference Proceedings IEEE Engineering in Medicine and Biology Society*, *2*(1), 1929–1932. Retrieved from http://www.ncbi.nlm.nih.gov/entrez/query.fcgi?cmd=Retrieve&db=PubMed&dopt=Citation&list_uids=17282598

Lesinski, S. G., Prewitt, J., Bray, V., Aravamudhan, R., Bermeo Blanco, O. A., Farmer-Fedor, B. L.,...,Ward, J. A. (2014). Preservation of auditory brainstem response thresholds after cochleostomy and titanium microactuator implantation in the lateral wall of cat scala tympani. *Otology & Neurotology*, *35*(4), 730–738. doi:10.1097/MAO.0000000000000281

Liu, L., Wang, H., Shi, L., Almuklass, A., He, T., Aiken, S.,...,Wang, J. (2012). Silent damage of noise on cochlear afferent innervation in guinea pigs and the impact on temporal processing. *PLoS One*, *7*(11), e49550doi:10.1371/journal.pone.0049550

Luo, C., Cao, G. Z., & Shen, I. Y. (2013). Development of a lead-zirconate-titanate (PZT) thin-film microactuator probe for intracochlear applications. *Sensors and Actuators A: Physical*, *201*, 1–9. doi:10.1016/j.sna.2013.06.027

Luo, C., Yang, C. W., Cao, G. Z., & Shen, I. Y. (2013). Effect of added mass on lead zirconate titanate (PZT) thin-film microactuators in aqueous environments. In: *Proceedings from ASME, Seventh International Conference on Micro- and Nanosystems*, Portland, OR.

Marsh, R. R., Yamane, H., & Potsic, W. P. (1981). Effect of site of stimulation on the guinea pig's electrically evoked brain stem response. *Otolaryngology–Head and Neck*

Surgery, *89*(1), 125–130. Retrieved from http://www.ncbi.nlm.nih.gov/entrez/query.fcgi?cmd=Retrieve&db=PubMed&dopt=Citation&list_uids=6784070

Mistry, N., Nolan, L. S., Saeed, S. R., Forge, A., & Taylor, R. R. (2014). Cochlear implantation in the mouse via the round window: Effects of array insertion. *Hearing Research*, *312*, 81–90. doi:10.1016/j.heares.2014.03.005

Nadol, J. B. J., Shiao, J. Y., Burgess, B. J., Ketten, D. R., Eddington, D. K., Gantz, B. J.,..., Shallop, J. K. (2001). Histopathology of cochlear implants in humans. *Annals of Otology, Rhinology & Laryngology*, *110*(9), 883–891. Retrieved from http://www.ncbi.nlm.nih.gov/entrez/query.fcgi?cmd=Retrieve&db=PubMed&dopt=Citation&list_uids=11558767

Nakajima, H. H., Merchant, S. N., & Rosowski, J. J. (2010). Performance considerations of prosthetic actuators for round-window stimulation. *Hearing Research*, *263*(1–2), 114–119. doi:10.1016/j.heares.2009.11.009

Ni, G., Elliott, S. J., Ayat, M., & Teal, P. D. (2014). Modelling cochlear mechanics. *BioMed Research International*, *2014*, 1–42. Retrieved from http://downloads.hindawi.com/journals/bmri/2014/150637.pdf

Noh, H., Abbas, P. J., Abbas, C. A., Nourski, K. V., Robinson, B. K.Jeng, F. C. (2007). Binaural interactions of electrically and acoustically evoked responses recorded from the inferior colliculus of guinea pigs. *International Journal of Audiology*, *46*(6), 309–320. doi:10.1080/14992020701212622

Oesterle, E. C., Sarthy, P. V., & Rubel, E. W. (1990). Intermediate filaments in the inner ear of normal and experimentally damaged guinea pigs. *Hearing Research*, *47*(1–2), 1–16.

O'Leary, S. J., Monksfield, P., Kel, G., Connolly, T., Souter, M. A., Chang, A.,..., Eastwood, H. (2013). Relations between cochlear histopathology and hearing loss in experimental cochlear implantation. *Hearing Research*, *298*, 27–35. doi:10.1016/j.heares.2013.01.012

Quesnel, A. M., Nadol, J. B., Gantz, B., Nakajima, H. H., & Roskowski, J. J. (2015). Loss of hearing following hearing preservation cochlear implantation with a hybrid device. *Otopathology Research Collaboration Network*, http://otopathologynetwork.org/educational-resources/webcasts/view/p20d5cyfzml/.

Reiss, L. A., Stark, G., Nguyen-Huynh, A. T., Spear, K. A., Zhang, H., Tanaka, C.,..., Li, H. (2015). Morphological correlates of hearing loss after cochlear implantation and electro-acoustic stimulation in a hearing-impaired Guinea pig model. *Hearing Research*, *327*, 163–174. doi:10.1016/j.heares.2015.06.007

Ren, T., He, W., & Gillespie, P. G. (2011). Measurement of cochlear power gain in the sensitive gerbil ear. *Nature Communications*, *2*, 216doi:10.1038/ncomms1226

Schraven, S. P., Mlynski, R., Dalhoff, E., Wildenstein, D., Alkonyi, B., Gummer, A. W.,..., Hagen, R. (2015). Vibro-EAS: A proposal for electroacoustic stimulation. *Otology & Neurotology*, *36*(1), 22–27. doi:10.1097/MAO.0000000000000593

Shi, L., Liu, L., He, T., Guo, X., Yu, Z., Yin, S.,..., Wang, J. (2013). Ribbon synapse plasticity in the cochleae of Guinea pigs after noise-induced silent damage. *PLoS One*, *8*(12), e81566. doi:10.1371/journal.pone.0081566

Sim, J. H., Röösli, C., Chatzimichalis, M., Eiber, A., & Huber, A. M. (2013). Characterization of stapes anatomy: Investigation of human and guinea pig. *Journal of the Association for Research in Otolaryngology*, *14*(2), 159–173. doi:10.1007/s10162-012-0369-5

Stover, T., & Lenarz, T. (2009). Biomaterials in cochlear implants. *GMS Current Topics in Otorhinolaryngology, Head and Neck Surgery*, *8*. Doc10. doi:10.3205/cto000062

Talbot, K. N., & Hartley, D. E. (2008). Combined electro-acoustic stimulation: A beneficial union. *Clinical Otolaryngology*, *33*(6), 536–545. doi:10.1111/j.1749-4486.2008.01822.x.

Tong, L., Strong, M. K., Kaur, T., Juiz, J. M., Oesterle, E. C., Hume, C.,..., Rubel, E. W. (2015). Selective deletion of cochlear hair cells causes rapid age-dependent changes in spiral ganglion and cochlear nucleus neurons. *Journal of Neuroscience*, *35*(20), 7878–7891. doi:10.1523/JNEUROSCI.2179-14.2015

Turner, C. W., & Gantz, B. J. (2012). Combining acoustic and electric hearing. In F. G. Zeng, A. N. Popper, & R. R. Fay (Eds.), *Auditory Prostheses: New Horizons* (pp. 59–84). New York, NY: Springer.

Woodson, E. A., Reiss, L. A., Turner, C. W., Gfeller, K., & Gantz, B. J. (2010). The Hybrid cochlear implant: A review. *Advances in Oto-Rhino-Laryngology*, *67*, 125–134. doi:10.1159/000262604

Yamane, H., Marsh, R. R., & Potsic, W. P. (1981). Brain stem response evoked by electrical stimulation of the round window of the guinea pig. *Otolaryngology–Head and Neck Surgery*, *89*(1), 117–124. Retrieved from http://www.ncbi.nlm.nih.gov/entrez/query.fcgi?cmd=Retrieve&db=PubMed&dopt=Citation&list_uids=6784069

Zeng, F. G., Rebscher, S., Harrison, W., Sun, X., & Feng, H. (2008). Cochlear implants: System design, integration, and evaluation. *IEEE Reviews in Biomedical Engineering*, *1*, 115–142. doi:10.1109/RBME.2008.2008250